Journal of Materials Chemistry A

Mechanochemistry-Driven Phase Transformation of Crystalline Covalent Triazine Frameworks Assisted by Alkaline Molten Salts

Journal:	*Journal of Materials Chemistry A*
Manuscript ID	TA-COM-03-2022-002117.R2
Article Type:	Communication
Date Submitted by the Author:	08-Jun-2022
Complete List of Authors:	Fan, Juntian; The University of Tennessee Knoxville, Chemistry Suo, Xian; University of Tennessee Knoxville Wang, Tao; Oak Ridge National Laboratory, Chemical Science Division Wang, Zongyu; ORNL Do-Thanh, Chi-Linh; UTK, Department of Chemistry Mahurin, Shannon; ORNL Kobayashi, Takeshi; U.S. DOE Ames National Laboratory, Yang, Zhenzhen; Oak Ridge National Laboratory, Chemical Science Division Dai, Sheng; ORNL

COMMUNICATION

Mechanochemistry-Driven Phase Transformation of Crystalline Covalent Triazine Frameworks Assisted by Alkaline Molten Salts

Received 00th January 20xx,
Accepted 00th January 20xx

DOI: 10.1039/x0xx00000x

Juntian Fan,[a] Xian Suo,[a] Tao Wang,[b] Zongyu Wang,[b] Chi-Linh Do-Thanh,[a] Shannon M. Mahurin,[b] Takeshi Kobayashi,[c] Zhenzhen Yang,*[,b] and Sheng Dai*[, a, b]

Covalent triazine frameworks (CTFs) have shown wide applications in the fields of separation, catalysis, energy storage, and beyond. However, it is a long-term challenging subject to fabricate high-quality CTF materials via facile procedures. Herein, a mechanochemistry-driven procedure was developed to achieve phase transformation of crystalline CTFs assisted by alkaline molten salts. The transformation of CTF-1 from staggered AB to eclipsed AA stacking mode was achieved by short time (30 min) mechanochemical treatment in the presence of molten salts composed of LiOH/KOH, generating high-quality CTF-1 material with high crystallinity, high surface area (625 m^2 g^{-1}), and permanent/ordered porosity without carbonization under ambient conditions. This facile procedure could be extended to provide nanoporous three-dimensional CTF materials.

Covalent triazine frameworks (CTFs) represent one of the most extensively developed nanoporous organic materials composed of light elements (C, N, and H).[1-5] The CTF skeletons linked by triazine units possess unique features including, but not limited to, full conjugation, permanent porosity, rich aza-fused functionalities, and the capability to tune the electronic/optic properties by structure design.[2, 4, 6-8] The merits of CTFs have been leveraged towards diverse applications in the field of adsorption, gas uptake, thermo/electro/photocatalysis, and energy storage.[3, 9-17]

There are mainly three approaches capable of constructing CTF skeletons via the triazine unit formation. Pathway I is the classical and most widely used ionothermal procedure promoted by $ZnCl_2$ with aromatic nitriles as the starting materials, affording CTFs via the trimerization of cyano groups.[1, 18-21] However, the relatively high reaction temperature (>400 °C), high loading amount of $ZnCl_2$ (1–10 equivalents), and long reaction time (up to 3 days) required in this approach always led to carbonized and semicrystalline or amorphous products. Later, a super Brønsted acid, trifluoromethanesulfonic acid (CF_3SO_3H), was demonstrated to act as an efficient catalyst for the CTFs construction from aromatic nitrile monomers in $CHCl_3$/CH_2Cl_2 solutions or under neat conditions assisted by thermal or microwave treatment, but still affording CTFs with low crystallinity in the form of powder or membrane.[22-27] Based on these advances, our group developed a transformation strategy to produce highly crystalline CTFs, in which CTF with staggered AB stacking mode was first constructed under low temperature (250 °C) ionothermal procedure catalyzed by CF_3SO_3H, and then thermal treatment under N_2 atmosphere (350 °C) could produce highly crystalline CTF with eclipsed AA stacking mode.[28] A recent progress made by Xu's group realized the synthesis of crystalline CTFs using the microwave-assisted strategy within a short time in the presence of a small amount of CF_3SO_3H.[29] Sulfur and lithium bis(trifluoromethanesulfonyl)imide (LiTFSI) were able to catalyze the trimerization of cyano groups towards CTF construction in battery-related applications, but the as-afforded materials are amorphous and doped with residual catalysts.[30, 31] Pathway II for CTF construction was through the trimerization of aromatic amide using an excess amount of P_2O_5 as the catalyst under relatively high temperature (400 °C), but still generated carbonized product.[32] Several solution-based methods (pathway III) have been developed for CTF synthesis using aromatic aldehydes and aromatic amidines as the monomers for the formation of triazine units via successive Schiff base formation and Michael addition catalyzed by inorganic base (e.g., Cs_2CO_3).[33] Then, aromatic alcohols or aromatic benzylic amines were used as the starting materials instead of aldehydes in the reaction to further improve the crystallinity of the materials.[34-36] However, requiring organic solvents and additional procedures on the monomer synthesis and purification hindered the scalability of these methods. There are also other approaches capable of producing triazine-

[a] Department of Chemistry, Institute for Advanced Materials and Manufacturing, University of Tennessee, Knoxville, TN 37996, USA
[b] Chemical Sciences Division, Oak Ridge National Laboratory, Oak Ridge, TN 37831, USA. Email: yangz3@ornl.gov; dais@ornl.gov
[c] U.S. DoE Ames Laboratory, Iowa State University, Ames, IA 50011, USA.
Electronic Supplementary Information (ESI) available: Experimental synthesis and characterization. See DOI: 10.1039/x0xx00000x

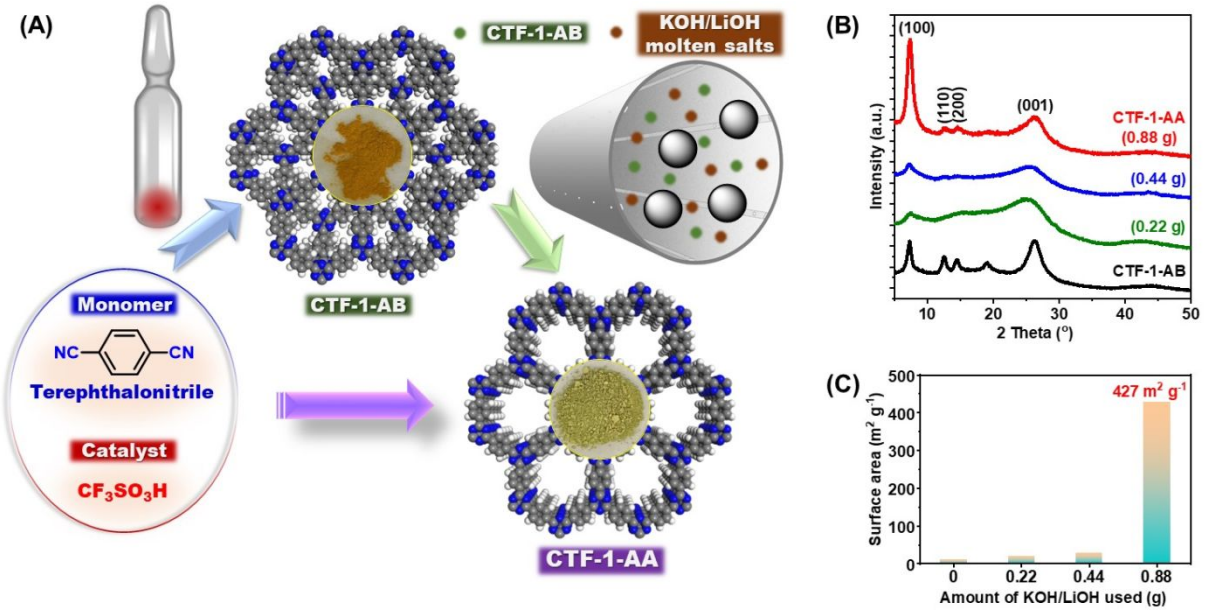

Figure 1 (A) Schematic illustration of the mechanochemistry-driven phase transformation of CTF-1-AB to CTF-1-AA assisted by KOH/LiOH molten salts. (B) XRD patterns and (C) BET surface areas of the CTF-1 materials obtained using different amounts of KOH/LiOH mixture in the ball milling procedure.

functionalized materials with monomers already containing triazine cores as the starting materials via diverse coupling reactions, but generally resulting in amorphous skeletons.[37-40] Although such progress has been made towards CTF construction, it is still highly desired to develop facile and easily accessible approaches capable of affording highly crystalline and non-carbonized CTF materials.

Herein, a mechanochemistry-driven procedure was developed to achieve the phase transformation of crystalline CTFs assisted by alkaline molten salts (Figure 1A). Taking CTF-1 from the polymerization of terephthalonitrile as an example, the transformation of CTF-1 from staggered AB stacking mode to eclipsed AA stacking mode was achieved by short time (30 min) ball milling treatment in the presence of molten salts composed of LiOH/KOH, generating high-quality CTF-1 material with high crystallinity, high surface area (625 m^2 g^{-1}), and permanent/ordered porosity without carbonization under ambient conditions. This facile mechanochemistry-driven and base-assisted procedure could be extended to the fabrication of three-dimensional (3D) CTF materials possessing ultra-microporous structures without carbonization, which were challenged to be obtained via the classical ionothermal pathway. The procedure developed in this work could realize the facile and rapid production of high-quality CTF materials without introducing carbonization, and this will provide extra opportunities to further extend the applications of these materials in catalysis and energy storage-related fields.

Previous work from our group revealed that the transformation of CTF-1 from staggered AB stacking mode to eclipsed AA stacking mode could be achieved by thermal treatment under N_2 atmosphere, producing highly crystalline material.[28] Related theoretical calculation results demonstrated that in CTF-1, the AA stacking order is more stable by 36 kJ mol^{-1} than the AB stacking order. In other words, the interlayer interaction is stronger in the AA stacking, partly due to its higher number of van der Waals contacts between atoms in the adjacent layers. However, a relatively high temperature of at least 350 °C was still required in this transformation procedure in order to break the strong interaction between the acid catalyst (CF_3SO_3H) and the as-formed triazine units, complete the twist of the CTF-1 layer into the eclipsed version, and build the permanent nanoporous channels with the CTF skeleton. It will be highly desired if such an AB-to-AA transformation could be achieved under ambient conditions to afford high-quality CTF materials with high crystallinity and abundant porosity. We envisaged that the addition of a properly selected base could help remove the residual strong acid catalyst and realize the AB-to-AA stacking mode transformation under mild conditions. Particularly, mechanochemistry could overcome the issues related to hazardous solvents utilization and high temperature procedures, and its sustainability and efficiency has been demonstrated in the fabrication of porous organic frameworks under neat conditions.[41-44] First, CTF-1 with AB stacking mode (denoted as CTF-1-AB) was synthesized via the previously reported ionothermal procedure at 250 °C using terephthalonitrile as the starting material and 50 mol% CF_3SO_3H as the catalyst (Figure 1A),[28] as demonstrated by the corresponding powder X-ray diffraction (PXRD) pattern (Figure 1B and Figure S1) and low surface area (Figure 1C). The XRD pattern of CTF-1-AB fit well with the simulated result, with the peaks located at 7.25, 12.58, 14.47, 19.01, and 26.29° showing up, which corresponded to the (100), (110), (200), (210), and (002) reflections, respectively.[45, 46] Before conducting the ball

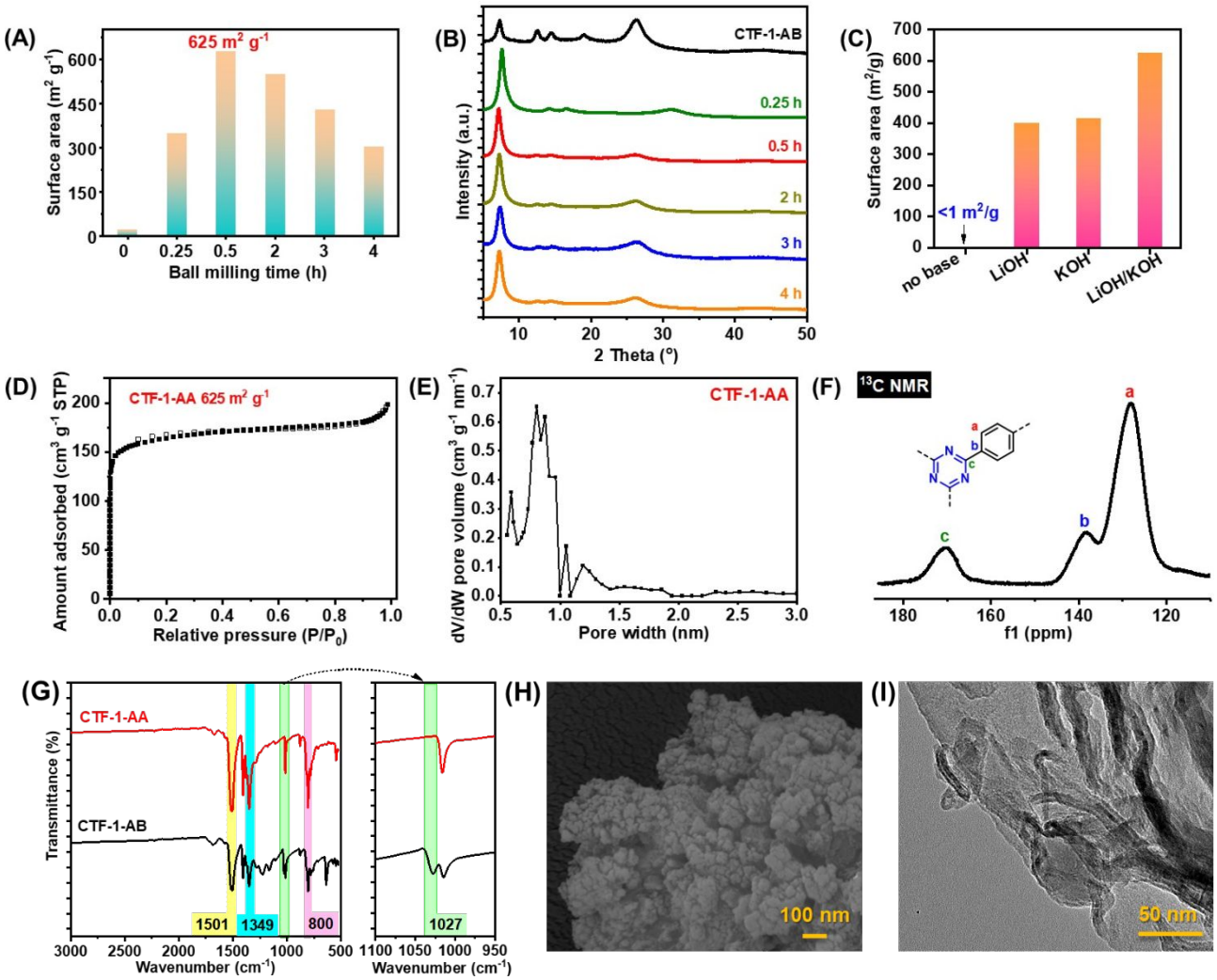

Figure 2 (A) BET surface areas and (B) PXRD patterns of the CTF-1 materials obtained by using different ball milling times in the presence of 0.88 g KOH/LiOH mixture. (C) BET surface areas of the CTF-1 materials obtained in the presence of molten salt (LiOH/KOH) mixture, LiOH, and KOH, respectively. Characterization of CTF-1-AA obtained by ball milling time of 30 min in the presence of 0.88 g LiOH/KOH mixture: (D) N_2 isotherms collected at 77 K, (E) NLDFT-derived pore size distribution curve, (F) solid-state ^{13}C NMR spectrum, (G) FTIR spectra, (H) SEM image, and (I) TEM image.

milling treatment, base-assisted thermal treatment of CTF-1-AB under nitrogen atmosphere was tested deploying an alkaline molten salt composed of KOH (68.6 mol%) and LiOH (31.4 mol%) owing to their low melting point (225 °C) (Figure S2) under the following condition: CTF-1-AB 0.2 g, LiOH + KOH mixture 0.88 g, 250 °C, 2 h. However, the precursor was decomposed with nothing being collected after the washing procedure. We envisaged that this was probably due to the strong basicity of the additive in its melting state (melting point: 225 °C). Therefore, a treatment procedure that can guarantee the sufficient contact and reaction of the base with the residual CF_3SO_3H under milder conditions was preferred. To test the feasibility of mechanochemistry-driven phase transformation of CTF-1-AB assisted by base, 0.2 g CTF-1-AB precursor (collected after the ionothermal procedure without further washing treatment) and a certain amount of the base mixture was placed in a stainless-steel reactor containing ball bearings, which was then treated by high-speed vibrating ball milling, and the product was collected and washed with water to remove the base additives. Both XRD patterns and surface areas of the as-afforded CTF-1 materials revealed that with the base amount gradually increasing from 0.22 to 0.88 g, the AB-to-AA stacking mode transformation was achieved under ambient conditions, and CTF-1-AA with significantly increased surface area (427 $m^2 g^{-1}$) was obtained (Figure S3-S4). Notably, XRD pattern of the as-obtained CTF-1-AA after ball milling with 0.88 g molten salt exhibited a predominant peak at 7.29°, being assigned to the (100) phase, together with small peaks at 12.65, 14.54, and 26.36° corresponding to the (110), (200), and (001) phase, respectively, which matched well with the simulated structure and XRD pattern of CTF-1 with AA stacking mode. The XRD evolution revealed that (Figure 1B), during the molten salt-assisted mechanochemical treatment, intensity of the peaks being assigned to the (110), (200), and (210) phase in AB

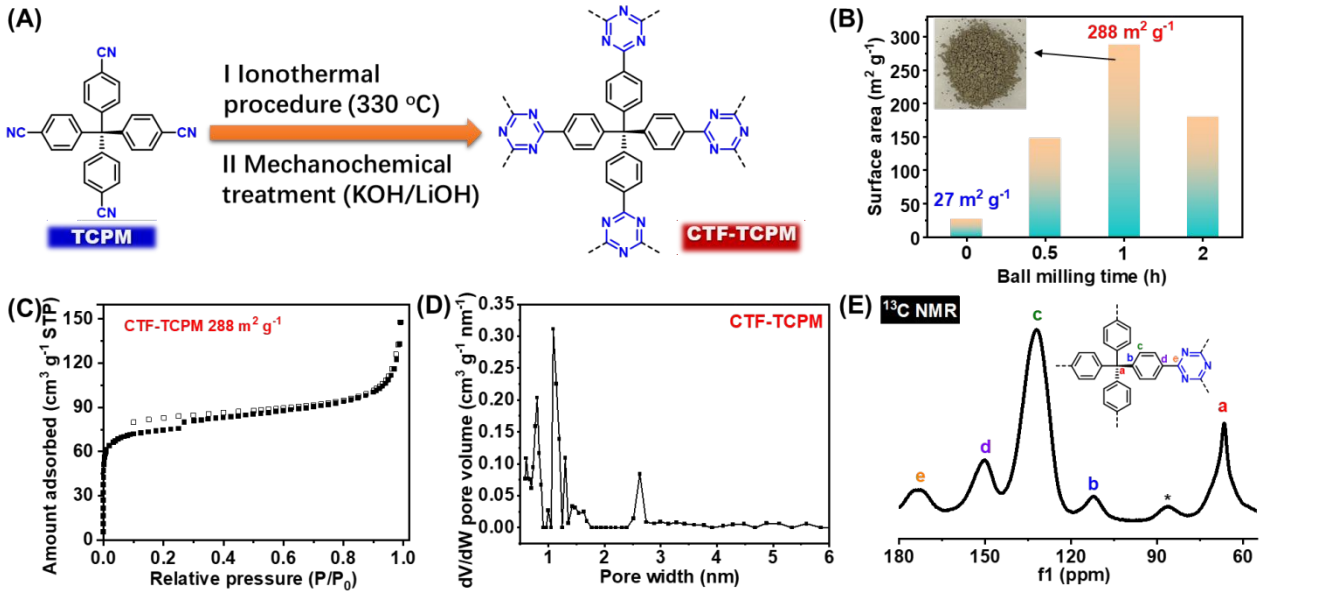

Figure 3 (A) Schematic illustration of the mechanochemistry-driven process to produce CTF-TCPM assisted by KOH/LiOH molten salts. (B) BET surface areas of the CTF-TCPM materials obtained using different ball milling times. Characterization of CTF-TCPM obtained by ball milling time of 1 h: (A) N_2 isotherms collected at 77 K, (B) Pore size distribution curve, and (C) solid-state ^{13}C NMR spectrum.

stacking gradually diminished. Comparatively, intensity of the peak belonging to in-plane (100) reflection at 2θ = 7.29° became more and more predominant, and in the simulated XRD pattern of CTF-1 with AA stacking mode, (100) phase was also the most predominant one. Correspondingly, the interlayer distance displayed almost no change, which was calculated to be ~3.4 Å from the peak of (001) crystal plane.

In order to further improve the quality of the CTF-1 materials, extensive studies were conducted on the influence of ball milling time and base. As shown in Figure 2A and 2B, a short ball milling time of 15 min could realize the AB-to-AA stacking mode transformation of CTF-1, and the surface area was increased to 348 $m^2\ g^{-1}$ (Figure S5). Further prolonging the ball milling time to 30 min could produce CTF-1-AA with a surface area of 625 $m^2\ g^{-1}$ (Figure 2D), which was comparable to the counterpart being generated by the high temperature thermal treatment method as well as the highly crystalline CTF-1 material produced via the microwave assisted procedure.[28, 29] However, further increasing the ball milling time (2 h, 3 h, and 4 h) led to diminished surface areas of the collected CTF materials, probably owing to the collapse of the porous structures during the high strength mechanochemical treatment process (Figure S4 and S6-S7). XRD patterns of the products demonstrated that all the CTF-1 products obtained with different ball milling time displayed a well-organized AA stacking mode structure (Figure 2B). Notably, if no base was added during the ball milling procedure, only nonporous product was obtained under the same mechanochemical treatment and washing procedure (Figure 2C). The merits of using the LiOH/KOH molten salt mixtures were revealed by the inferior surface areas of the CTF-1 product obtained in the presence of only KOH or LiOH (Figure S8 and S9), which had relatively high melting points (Figure S2). A control experiment involving the addition of a trace amount of water during the mechanochemical treatment procedure revealed that water has no significant influence on the XRD pattern and surface area of the as-afforded CTF product (Figure S10).

Detailed characterizations of the CTF-1-AA with surface area of 625 $m^2\ g^{-1}$ were conducted to provide more detailed structure information. N_2 adsorption and desorption isotherms of CTF-1-AA collected at 77 K exhibited a typical type I feature, with rapid uptake capacity increase in the low-pressure region (< 0.1 bar), indicating the micropore structure (Figure 2D). The non-local density functional theory method (NLDFT)-derived pore size distribution curve further demonstrated the presence of micropores in the skeleton around 1.1 nm, which corresponded to the unit size of the CTF-1 structure, and extra ultra-micropores (0.5–1 nm) introduced during the alkaline base-assisted ball milling procedure (Figure 2E and S11), which will provide more benefits in gas separation-related ap plications.[11]

Solid-state cross-polarization magic-angle spinning ^{13}C nuclear magnetic resonance (SS CP/MAS ^{13}C NMR) analysis confirmed the construction of triazine-linked scaffolds in CTF-AA, with three major peaks with chemical shift values of 128 (peak a) and 138 ppm (peak b) for benzene rings and 170 ppm (peak c) for triazine rings (Figure 2F).[2] Fourier-transform infrared (FTIR) spectroscopy demonstrated that the triazine linkage was already formed in CTF-1-AB and maintained well in CTF-1-AA, with characteristic peaks located at 800, 1349 and 1501 cm^{-1} (Figure 2G).[5, 6] CTF-1 obtained from the CF_3SO_3H-catalyzed ionothermal procedure without any washing exhibited obvious S=O symmetric stretching vibrations from CF_3SO_3H at 1027 cm^{-1}, which completely disappeared after the alkaline molten salts-assisted mechanochemical treatment.[45]

Thermogravimetric analysis (TGA) revealed promising stability of the as-afforded CTF-1-AA products, with onset decomposition temperatures of 640 and 510 °C under nitrogen and air atmosphere, respectively (Figure S12), making them promising materials in high-temperature gas adsorption and catalysis. Room temperature electron spin resonance (ESR) of CTF-1-AA indicated the existence of unpaired electrons within the skeletons derived from the abundant nitrogen-containing species (Figure S13). Scanning electron microscopy (SEM) and transmission electron microscopy (TEM) images of CTF-1-AA indicated that the as-produced material was composed of particles with stripy and thin layered structures (Figure 2H and 2I).

Then, the mechanochemistry-driven procedure was deployed to fabricate CTFs with 3D structure and permanent porosity, which was more challenging to achieve using the classical ionothermal procedure promoted by $ZnCl_2$, and only carbonized products can be obtained.[47, 48] Tetrakis(4-cyanophenyl)methane (TCPM) was used as the starting material (Figure 3A). First, the trimerization of the monomers was conducted using 50 mol% CF_3SO_3H as the catalyst under neat conditions. The heating temperature was determined as 330 °C, which was a little bit higher than the melting point of TCPM (312 °C). Then, the as-collected product with surface area of 26 $m^2 g^{-1}$ (Figure S14) was treated by ball milling in the presence of KOH/LiOH molten salt, and the generated CTF products were denoted as CTF-TCPM. Detailed study on the ball milling time revealed that CTF-TCPM with an optimal surface area of 288 $m^2 g^{-1}$ could be obtained with treatment time of 1 h (Figure 3B, 3C, and Figure S15-S16). Notably, the product was collected as a greenish powder without carbonization (Figure 3B). The N_2 isotherm of CTF-TCPM exhibited the typical type I feature (Figure 3C), indicating the porous structures were mainly contributed by micropores. Accordingly, the pore size distribution curve of CTF-TCPM confirmed that the porous structure was mainly composed of ultra-micropore (~0.8 nm) and micropore (1.1 nm), together with small amounts of mesopores (~2.6 nm). However, XRD patterns of the CTF-TCPM precursors and the as-obtained products after KOH/LiOH-assisted mechanochemical treatment revealed that these architectures are amorphous (Figure S17), and no significant changes were observed in the XRD results. Notably, it was demonstrated that in CTF-1 systems,[49] the CF_3SO_3H dimer (acid catalyst) being trapped in the interlayer space could form strong hydrogen bonds with the triazine and benzene rings in adjacent layers, leading to the favorable formation of AB stacking. In the CTF-TCPM system, although the architectures are amorphous, the removal of the residual CF_3SO_3H driven by the neutralization reaction with the added base during the ball milling procedure could also lead to rearrangement of the skeletons without the hydrogen bonding formation, which was like the removal of the guest molecules from a fitted pores/window. Therefore, the improvement of the surface area/porosity of the CTF-TCPM was derived from the removal of the residual CF_3SO_3H moieties, which could block the pores, and the rearrangement of the skeletons without the constraint from the hydrogen bonding formation. The FTIR spectrum of CTF-TCPM obtained after ball milling of 1 h in the presence of LiOH/KOH showed characteristic peaks of triazine linkages (800, 1349 and 1501 cm^{-1}) and benzene rings (1606, 1411, 1017, 823 cm^{-1}) (Figure S18). SS CP/MAS ^{13}C NMR further confirmed that the CTF-TCPM scaffold was constructed by a tertiary central carbon (peak a, 67 ppm), benzene rings (peak b, c, and d, 112-151 ppm), and triazine linkages (peak e, 173 ppm). Therefore, the combination of ionothermal and mechanochemical procedures developed herein will enable us to produce CTFs with diverse structures and properties.

Conclusions

Towards the construction of high-quality CTF materials via facile procedures, a mechanochemistry-driven procedure was developed. Successful phase transformation of CTFs was achieved under ambient conditions assisted by alkaline molten salts to generate CTF materials with high crystallinity, high surface area, and permanent porosity. This method will provide extra opportunities to extend the applications of the CTF materials in the field of catalysis, energy storage, and beyond.

Acknowledgements

The research was supported financially by the Division of Chemical Sciences, Geosciences, and Biosciences, Office of Basic Energy Sciences, US Department of Energy. Work at the Ames Laboratory (solid-state NMR) was supported by the Department of Energy-Basic Energy Sciences under Contract No. DE-AC02-07CH11358.

Conflicts of interest

There are no conflicts to declare.

Notes and references

1. P. Kuhn, M. Antonietti and A. Thomas, *Angew. Chem. Int. Ed.*, 2008, **47**, 3450-3453.
2. Y. Zhang and S. Jin, *Polymer*, 2018, **11**, 31-47.
3. P. Puthiaraj, Y.-R. Lee, S. Zhang and W.-S. Ahn, *Journal of Materials Chemistry A*, 2016, **4**, 16288-16311.
4. C. Krishnaraj, H. S. Jena, K. Leus and P. Van Der Voort, *Green Chem.*, 2020, **22**, 1038-1071.
5. H. Chen, X. Suo, Z. Yang and S. Dai, *Adv. Mater.*, 2021, DOI: 10.1002/adma.202107947, e2107947.
6. M. Liu, L. Guo, S. Jin and B. Tan, *J. Mater. Chem. A*, 2019, **7**, 5153-5172.
7. X. Suo, F. Zhang, Z. Yang, H. Chen, T. Wang, Z. Wang, T. Kobayashi, C. L. Do-Thanh, D. Maltsev, Z. Liu and S. Dai, *Angew. Chem. Int. Ed.*, 2021, **60**, 25688-25694.
8. Z. Yang, S. Wang, Z. Zhang, W. Guo, K. Jie, M. I. Hashim, O. Š. Miljanić, D.-e. Jiang, I. Popovs and S. Dai, *J. Mater. Chem. A*, 2019, **7**, 17277-17282.
9. M. Sun, S. Han, J. Feng, C. Li, X. Ji, J. Feng and H. Sun, *Top. Curr. Chem.*, 2021, **379**, 24.
10. Q. W. Deng, G. Q. Ren, Y. J. Li, L. Yang, S. L. Zhai, T. Yu, L.

Sun, W. Q. Deng, A. Li and Y. H. Zhou, *Mater. Today Energy*, 2020, **18**, 100506.
11. H. Wang, D. Jiang, D. Huang, G. Zeng, P. Xu, C. Lai, M. Chen, M. Cheng, C. Zhang and Z. Wang, *J. Mater. Chem. A*, 2019, **7**, 22848-22870.
12. S. Hug, L. Stegbauer, H. Oh, M. Hirscher and B. V. Lotsch, *Chem. Mater.*, 2015, **27**, 8001-8010.
13. Z. Qian, Z. J. Wang and K. A. I. Zhang, *Chem. Mater.*, 2021, **33**, 1909-1926.
14. C. B. Meier, R. Clowes, E. Berardo, K. E. Jelfs, M. A. Zwijnenburg, R. S. Sprick and A. I. Cooper, *Chem. Mater.*, 2019, **31**, 8830-8838.
15. X. Jiang, P. Wang and J. Zhao, *J. Mater. Chem. A*, 2015, **3**, 7750-7758.
16. Z. Yang, T. Wang, H. Chen, X. Suo, P. Halstenberg, H. Lyu, W. Jiang, S. M. Mahurin, I. Popovs and S. Dai, *ACS Energy Letters*, 2021, **6**, 41-51.
17. H. Chen, Z. Yang, C. L. Do-Thanh and S. Dai, *ChemSusChem*, 2020, **13**, 6182-6200.
18. M. J. Bojdys, J. Jeromenok, A. Thomas and M. Antonietti, *Adv. Mater.*, 2010, **22**, 2202-2205.
19. P. Katekomol, J. Roeser, M. Bojdys, J. Weber and A. Thomas, *Chem. Mater.*, 2013, **25**, 1542-1548.
20. A. Bhunia, V. Vasylyeva and C. Janiak, *Chem. Commun.*, 2013, **49**, 3961-3963.
21. H. Ren, T. Ben, E. Wang, X. Jing, M. Xue, B. Liu, Y. Cui, S. Qiu and G. Zhu, *Chem. Commun.*, 2010, **46**, 291-293.
22. S. Ren, M. J. Bojdys, R. Dawson, A. Laybourn, Y. Z. Khimyak, D. J. Adams and A. I. Cooper, *Adv. Mater.*, 2012, **24**, 2357-2361.
23. X. Zhu, C. Tian, S. M. Mahurin, S.-H. Chai, C. Wang, S. Brown, G. M. Veith, H. Luo, H. Liu and S. Dai, *J. Am. Chem. Soc.*, 2012, **134**, 10478-10484.
24. J. Liu, W. Zan, K. Li, Y. Yang, F. Bu and Y. Xu, *J. Am. Chem. Soc.*, 2017, **139**, 11666-11669.
25. J. Liu, P. Lyu, Y. Zhang, P. Nachtigall and Y. Xu, *Adv. Mater.*, 2018, **30**, 1705401.
26. Z. Yang, T. Liu, S. Wang, H. Chen, X. Suo, T. Wang, B. P. Thapaliya, D.-e. Jiang, I. Popovs and S. Dai, *Chem. Mater.*, 2021, **33**, 3386-3393.
27. Z. Yang, W. Guo, S. M. Mahurin, S. Wang, H. Chen, L. Cheng, K. Jie, H. M. Meyer, III, D.-e. Jiang, G. Liu, W. Jin, I. Popovs and S. Dai, *Chem*, 2020, **6**, 631-645.
28. Z. Yang, H. Chen, S. Wang, W. Guo, T. Wang, X. Suo, D. E. Jiang, X. Zhu, I. Popovs and S. Dai, *J. Am. Chem. Soc.*, 2020, **142**, 6856-6860.
29. T. Sun, Y. Liang and Y. Xu, *Angew Chem Int Ed Engl*, 2021, DOI: 10.1002/anie.202113926.
30. S. N. Talapaneni, T. H. Hwang, S. H. Je, O. Buyukcakir, J. W. Choi and A. Coskun, *Angew. Chem. Int. Ed.*, 2016, **55**, 3106-3111.
31. T. Zhou, Y. Zhao, J. W. Choi and A. Coskun, *Angew. Chem. Int. Ed.*, 2019, **58**, 16795-16799.
32. S. Y. Yu, J. Mahmood, H. J. Noh, J. M. Seo, S. M. Jung, S. H. Shin, Y. K. Im, I. Y. Jeon and J. B. Baek, *Angew. Chem. Int. Ed.*, 2018, **57**, 8438-8442.
33. K. Wang, L.-M. Yang, X. Wang, L. Guo, G. Cheng, C. Zhang, S. Jin, B. Tan and A. Cooper, *Angew. Chem. Int. Ed.*, 2017, **56**, 14149-14153.
34. M. Liu, Q. Huang, S. Wang, Z. Li, B. Li, B. Tan and S. Jin, *Angew. Chem. Int. Ed.*, 2018, **57**, 11968-11972.
35. M. Liu, K. Jiang, X. Ding, S. Wang, C. Zhang, J. Liu, Z. Zhan, G. Cheng, B. Li, H. Chen, S. Jin and B. Tan, *Adv. Mater.*, 2019, **31**, e1807865.
36. S. Zhang, G. Cheng, L. Guo, N. Wang, B. Tan and S. Jin, *Angew. Chem. Int. Ed.*, 2020, **59**, 6007-6014.
37. P. Puthiaraj, S.-M. Cho, Y.-R. Lee and W.-S. Ahn, *J. Mater. Chem. A*, 2015, **3**, 6792-6797.
38. E. Troschke, S. Grätz, T. Lübken and L. Borchardt, *Angew. Chem. Int. Ed.*, 2017, **56**, 6859-6863.
39. W. Huang, B. Li, Y. Wu, Y. Zhang, W. Zhang, S. Chen, Y. Fu, T. Yan and H. Ma, *ACS Appl. Mater. Interfaces*, 2021, **13**, 13604-13612.
40. P. Puthiaraj, S.-S. Kim and W.-S. Ahn, *Chem. Eng. J.*, 2016, **283**, 184-192.
41. P. Zhang, H. Li, G. M. Veith and S. Dai, *Adv. Mater.*, 2015, **27**, 234-239.
42. P. Zhang, X. Jiang, S. Wan and S. Dai, *J. Mater. Chem. A*, 2015, **3**, 6739-6741.
43. B. P. Biswal, S. Chandra, S. Kandambeth, B. Lukose, T. Heine and R. Banerjee, *J. Am. Chem. Soc.*, 2013, **135**, 5328-5331.
44. S. Chandra, S. Kandambeth, B. P. Biswal, B. Lukose, S. M. Kunjir, M. Chaudhary, R. Babarao, T. Heine and R. Banerjee, *J. Am. Chem. Soc.*, 2013, **135**, 17853-17861.
45. Z. Yang, H. Chen, S. Wang, W. Guo, T. Wang, X. Suo, D.-e. Jiang, X. Zhu, I. Popovs and S. Dai, *J. Am. Chem. Soc.*, 2020, **142**, 6856-6860.
46. J. Liu, P. Lyu, Y. Zhang, P. Nachtigall and Y. Xu, *Adv. Mater.*, 2018, **30**, 1705401.
47. S. Dey, A. Bhunia, I. Boldog and C. Janiak, *Micropor. Mesopor. Mater.*, 2017, **241**, 303-315.
48. X. Zou, H. Ren and G. Zhu, *Chem. Commun.*, 2013, **49**, 3925-3936.
49. Y. Qu, F.-X. Sauvage, G. Clavier, F. Miomandre and P. Audebert, *Angew. Chem. Int. Ed.*, 2018, **57**, 12057-12061.